Integrating Comprehensive Two-Dimensional Gas Chromatography and Downhole Fluid Analysis to Validate a Spill-Fill Sequence of Reservoirs with Variations of Biodegradation, Water Washing and Thermal Maturity

Jerimiah C. Forsythe[1], Robin Martin,[2] Ilaria De Santo,[3] Richard Tyndall,[2] Kate Arman,[2] Jonathan Pye,[2] Nelly De Nicolais,[3] Robert K. Nelson,[4] Andrew E. Pomerantz,[1] Stephen Kenyon-Roberts,[2] Julian Y. Zuo,[5] Christopher Reddy,[4] Kenneth Peters,[6] Oliver C. Mullins[1]

1. Schlumberger-Doll Research, 2. Premier Oil Company, 3. Schlumberger Wireline UK, 4 Woods Hole Oceanographic Institution, 5. Schlumberger HPS, 6. Schlumberger SIS

Abstract

Optimization of crude oil production depends heavily on crude oil composition and its variation within individual reservoirs and across multiple reservoirs. In particular, asphaltene content has an enormous impact on crude oil viscosity and even the economic value of the fluids in the reservoir. Thus, it is highly desirable to understand the primary controls on crude oil composition and asphaltene distributions in reservoirs. Here, a complex oilfield in the North Sea containing six separate reservoirs is addressed. The crude oil is believed to have spilled out of deeper reservoirs into shallower reservoirs during the overall reservoir charging process. Asphaltene content is measured *in-situ* through downhole fluid analysis and is generally consistent with a spill-fill sequence in reservoir charging. Detailed compositional analysis of crude oil samples by comprehensive two-dimensional gas chromatography (GC×GC) is used to determine the extent and variation among the reservoirs of water washing, biodegradation and thermal maturity. Increased biodegradation and water washing in the shallower reservoirs is consistent with a spill-fill sequence. The water washing is evidently assisted by biodegradation. Moreover, analyses of four thermal maturity biomarkers show that shallower reservoirs contain less mature oil, again consistent with a spill-fill sequence. The combination of DFA for bulk compositional analysis and GC×GC for detailed compositional analysis with geochemical interpretation is an effective tool for unraveling complex oilfield scenarios.

Introduction

Reservoir crude oils can vary widely in composition, thus physical properties can vary spatially within reservoirs and across multiple reservoirs in an oilfield. In particular, crude oils contain dissolved gas, liquids and dissolved solids, the asphaltenes. All potential phase transitions of crude oils are important for constraining production parameters such as the bubble (or dew) point, asphaltene onset and wax appearance temperature. The mass fractions of these bulk components have significant impact on the value of the crude oil as well as on optimal methods of production. Crude oils of high gas-oil ratio (GOR) are rather compressible thereby aiding in pressure maintenance during production. However, these oils necessitate treatment of high pressure gas in surface facilities for production. High asphaltene content of crude oils lowers

economic value; the low H:C ratios of asphaltenes of about 1 limit the ability to generate liquid fuels which have H:C ratios of about 2. In addition, the viscosity of crude oils depends exponentially on asphaltene content hindering production of oils with high asphaltene content. It is important to understand crude oil properties not only at the point of sample acquisition in the wellbore but also at locations far from the wellbore.

In many cases, there are considerable vertical and lateral variations of crude properties in individual reservoirs. These variations can often be associated with dynamic processes that crude oils undergo in geologic time.[Mullins et al, 2014] It is highly desirable to understand these dynamic processes in order to extrapolate oil properties away from the wellbore where fluid samples are acquired. An example of an integrated analysis is shown below for the Bhagyam reservoir in the Rajasthan basin, India.[Zuo et al, 2015] A large, disequilibrium gradient of asphaltenes exists in the oilfield as shown in Fig. 1. This oil reservoir is very shallow, a few hundred meters deep, thus is cold and expected to be undergoing biodegradation. The reservoir was charged about 50 million years ago (in the Eocene Epoch). Fig 1A shows the measurement of asphaltene content vs true vertical depth using downhole fluid analysis (DFA).[Mullins, 2008] Also shown in the gas chromatography (GC) that towards the base of the oil column, the alkanes are diminished, while towards the top of the oil column, the *n*-alkanes are present and clearly seen as a series of large spikes in the GC. [Zuo et al, 2015] Clearly, the alkane distribution is not equilibrated in this oil column; equilibration of *n*-alkanes would correspond to a much more homogeneous distribution than observed. Also, the drilling fluid filtrate contamination is evident towards the base of the oil column where the oils are enriched in asphaltene, more viscous and harder to sample without filtrate contamination.

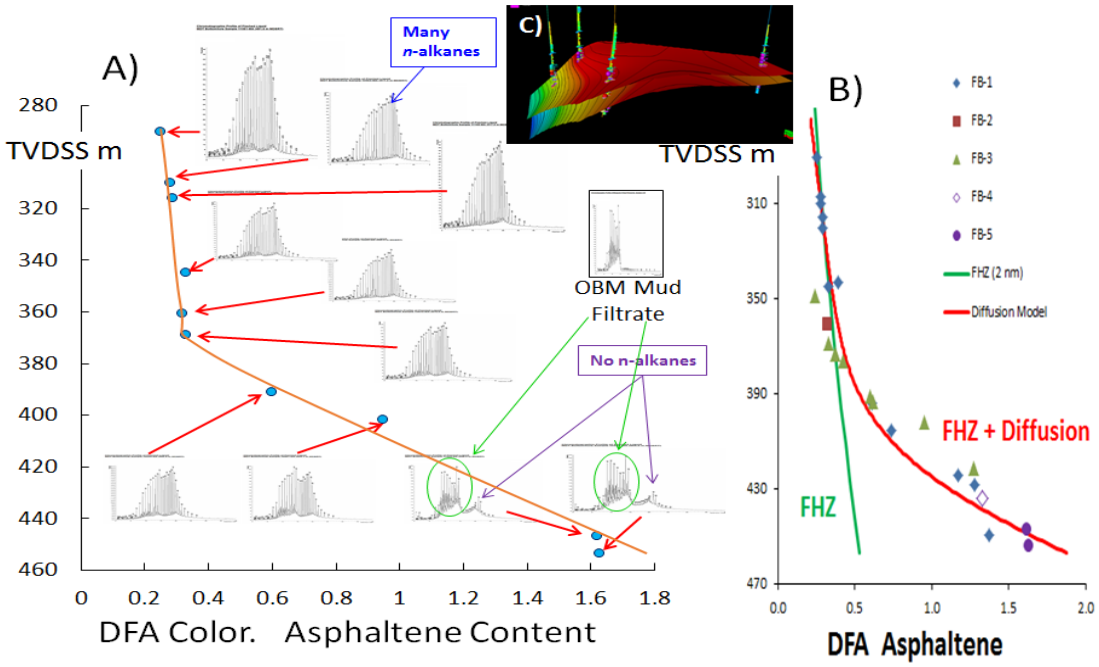

Figure 1. Fluid gradients from the Bhagyam reservoir.[Zuo et al, 2015] A) Asphaltenes versus

depth (true vertical depth, subsea) along with gas chromatograms (GCs) of the oil samples. B) Asphaltene gradient data fit with the FHZ EoS and the FHZ EoS plus a diffusive term accounting for the effects of alkane diffusion to the oil-water contact with subsequent removal by biodegradation. An asphaltene nanoaggregate size of 2.0 nm is used from the Yen-Mullins model.

Figure 1B shows the DFA-measured asphaltene gradients fit with two different theoretical expressions. The fit with the Flory-Huggins-Zuo equation of state (FHZ EoS) [Freed et al; Zuo et al, 2013] using the 2nm asphaltene nanoaggregate from the Yen-Mullins model [Mullins, 2010] works only for the upper half of the oil column but does not fit the lower half of the oil column due to ongoing biodegradation. That is, because the FHZ EoS is static (no time dependence) yet the oil column is undergoing active biodegradation, a dynamic term needs to be included. Biodegradation occurs at the oil-water contact (OWC) at the base of the oil column.[Head et al, 2003] The microbes live in the water and preferentially consume alkanes [Peters et al, 2005] thereby explaining the lack of *n*-alkanes in the GCs at the base of the oil column. *n*-Alkanes originating higher in the oil column can diffuse to the OWC and get consumed. The model FHZ+Diffusion incorporates these dynamics and is shown to fit the asphaltene gradient very well in Fig. 1B.[Zuo et al, 2015] The microbes can consume at most 2/3 of the oil [Head et al, 2003] thus extensive biodegradation can yield a tripling of the asphaltene content beyond what it would have been in unperturbed crude oil. Fig. 1B shows just this tripling of asphaltene content at the base of the oil column. As time progresses, diffusion reaches higher up the oil column. The duration of the diffusive model shown in Fig. 1B is 50 million years matching the start of reservoir charging obtained from petroleum system modeling of the Bhagyam reservoir.[Zuo et al, 2015]

In some reservoirs, more complex process can occur. In the Llanos basin, in Colombia in the eastern forelands of the Andes, reservoirs can undergo biodegradation, multiple charging and water washing. To unravel these complexities, GCxGC is quite useful. Fig. 2 shows a GCxGC chromatogram from an oil obtained from a reservoir in Llanos basin.

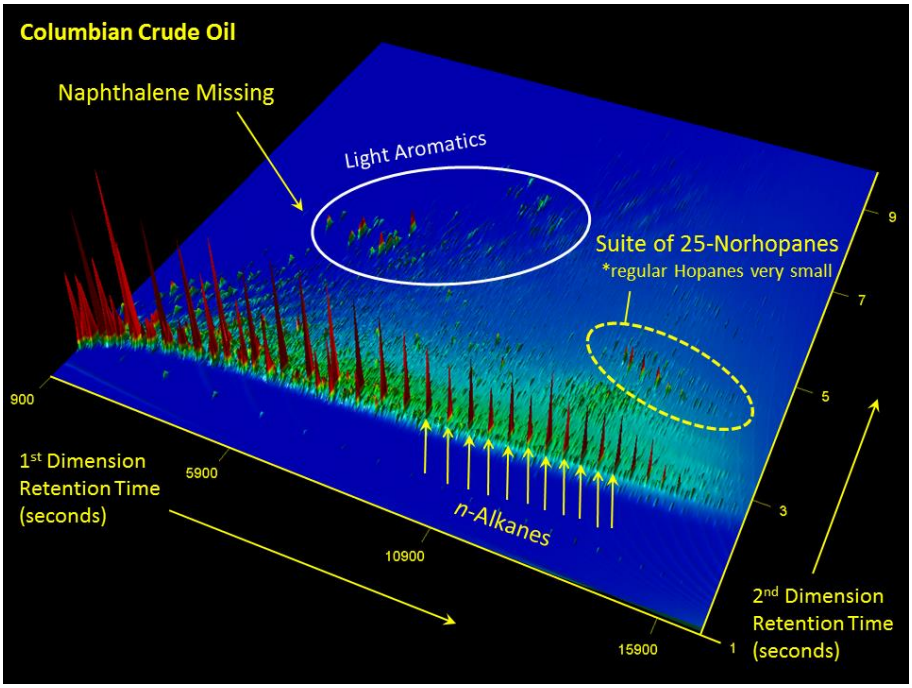

Figure 2. GCxGC chromatogram from a crude oil from Llanos Basin.[Bartha et al, 2015] The absence of the relatively water soluble naphthalene is likely from water washing consistent with the very active aquifer in the Llanos basin. The relative abundance of 25-norhopanes over corresponding hopanes indicates extensive biodegradation of 6 on the Peters-Moldowan scale.[Peters et al, 2005] The presence of n-alkanes indicates a second unbiodegraded charge of oil into the reservoir.[Bartha et al, 2015]

Figure 2 indicates the abundance of 25-norhopanes over the corresponding hopanes, thus extensive biodegradation occurred. This corresponds to a level of 6 on the Peters-Moldowan scale.[Peters et al, 2005] At this level, the *n*-alkanes are entirely consumed. Cleary, *n*-alkanes are present in this oil in Fig. 2. This indicates that the oil reservoir had two oil charges, the first charge underwent extensive biodegradation yielding 25-norhopanes. The second charge was not biodegraded at all. As shown in petroleum system modeling,[Bartha et al, 2015] between the first and second oil charges, the reservoir subsided and heated to temperatures beyond survival of the microbes (~85^{o}C). Consequently, the second oil charge remained unbiodegraded and thus much better oil quality. Petroleum system modeling shows that some reservoirs in the Llanos basin likely heated beyond biodegradation temperatures prior to much oil charging thereby preserving unbiodegraded oil which has much better value.[Bartha et al, 2015]

Figure 2 shows a good separation of light aromatics, which can be used to assess water washing. In particular, naphthalene is absent while methyl naphthalenes are present. Figure 3 shows an expanded view of this region of the GCxGC chromatogram for two crude oils from a reservoir in the Llanos basin.

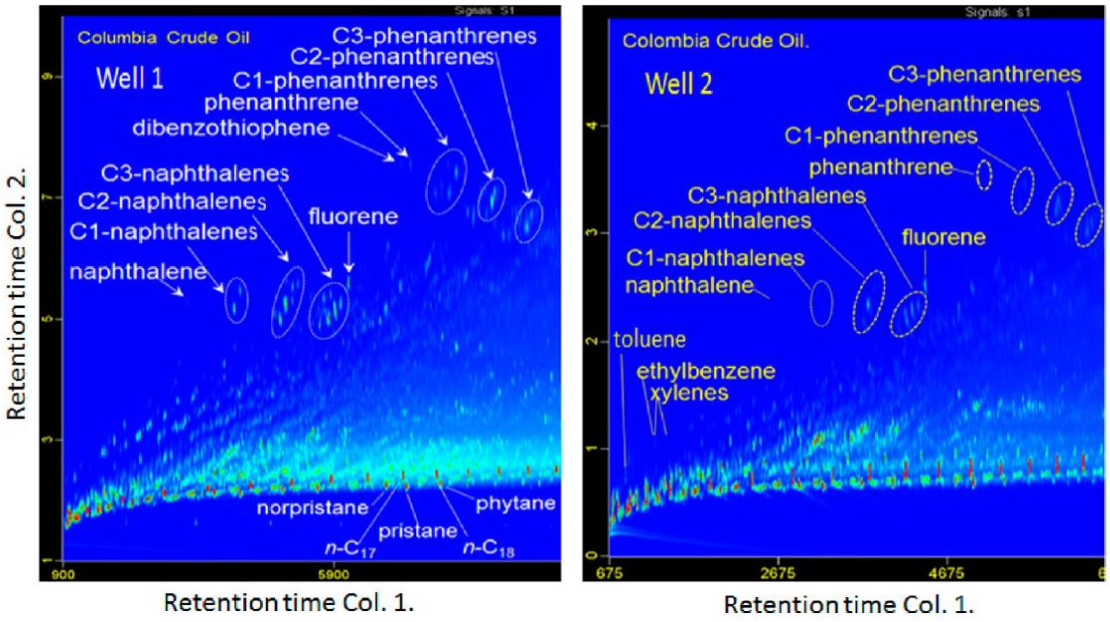

Figure 3. Two oils from different lateral positions in the same reservoir in the Llanos Basin. The extent of water washing differs somewhat in the two oils with differing reductions of lower molecular weight alkylnaphthalenes in crude oils from Well 1 and Well 2. [Bartha et al, 2015]

Other studies have combined DFA and GCxGC for a variety of purposes including reservoir compartmentalization [Mullins, 2008] and connectivity, [Mullins, 2008; Pomerantz et al, 2010; Dong et al, 2014; Forsythe et al, 2015] multiple charging [Pomerantz et al, 2010] and analysis of tar mat formation [Forsythe et al, 2015]. This combination is effective for evaluation of many reservoir concerns.

In this study herein, crude oils from six reservoirs in the Catcher Area Field in the Central North Sea, UK, are analyzed particularly with regard to the possible spill-fill scenario of reservoir charging. DFA data regarding asphaltene content is analyzed to check for consistency with this concept. Detailed compositional analyses of the crude oils by GCxGC with geochemical interpretation indicate that significantly different levels of biodegradation and water washing are present in these crude oils. In addition, four different thermal maturity biomarkers are analyzed and show consistent and systematic variations. All chemical analyses performed here support the spill-fill scenario for these six reservoirs.

2. Methodology

Wireline Sampling Acquisition and Analysis.

Fourteen samples of crude oil acquired in six wells at various depths have been analysed. The samples were acquired using the openhole wireline formation sampling tool, the Modular Formation Dynamics Tester (MDT). The samples were flashed to remove volatile components (<*n*-C_5). The flashed whole crude oil samples were used in all gas chromatography experiments with each sample diluted to 100 mg mL^{-1} in methylene chloride.

Wireline sample acquisition can be challenging due to the viscous nature of oils and the presence of an active aquifer. Additionally, in open-hole sample acquisition, it is necessary to pump for long periods of time to reduce contamination from drilling fluid filtrate that penetrates oil-bearing formations. Figure 4 depicts the MDT, which is a complex instrument package consisting of several components or modules, such as pumps, fluid analyzers, and sample bottles that is lowered into the well on a cable or "wireline". The MDT is configured to have one or more probe modules which establish hydraulic communication with permeable formations. One type of probe is shown in Fig. 4; the single probe has a stout, steel tube. This tube, along with a surrounding packer, is pressed against the formation wall with great force to create a seal. The onboard pumps on the MDT lower the pressure in the flow line, enabling extraction of fluids from the permeable formation.

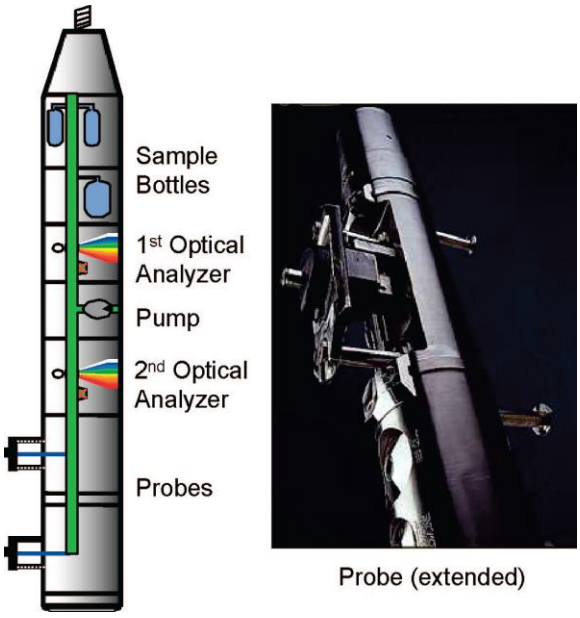

Figure 4. Schematic diagram of a wireline sampling tool, the "MDT" which acquires crude oil samples from wells.[Mullins, 2008] Modules on the MDT perform optical spectroscopy and other measurements on samples for in-situ chemical analysis. This tool is used in so-called "open hole" just after the well is drilled and prior to placement of steel casing in the well. A photograph of a type of "probe" is shown with a thick-walled, steel tube which is pressed firmly against the borehole wall along with a packer to make hydraulic communication with permeable zones. With the MDT pump, the pressure is reduced in the flowline, and fluids flow from the formation into the tool. DFA enables characterization of the fluid contents of the flowline; when clean formation fluids are flowing, high pressure sample bottles on the MDT can be opened to acquire formation fluid samples for subsequent study.

The MDT enables acquisition of representative samples of formation fluids from open hole wells. The provenance of crude oil samples in a reservoir is recorded with great accuracy within the well, an essential component for evaluation of the crude oil within a thermodynamic context where fluid gradient analysis is critical. Downhole fluid analysis (DFA) allows analysis thus minimization of contamination of the crude oil by drilling mud filtrate that penetrates into oil-

bearing formations by optimized pumping times. The DFA tool of choice is the IFA (cf. Fig. 5) which can monitor possible phase transitions, such as gas evolution that can destroy the validity of crude oil samples; this phase transition can be avoided by measurement of flow line contents and adjusting flow line pressure accordingly. In addition, the near infra-red measurements of IFA enable quantification of oil, water, and gas fractions. Thus, the IFA allows for determination of crude oil and water fractions in the flow line, so that optimal pumping times for sample acquisition can be employed. Additionally, IFA measures crude oil density and viscosity at reservoir conditions. Figure 5 shows an image of the IFA with its many sensors.

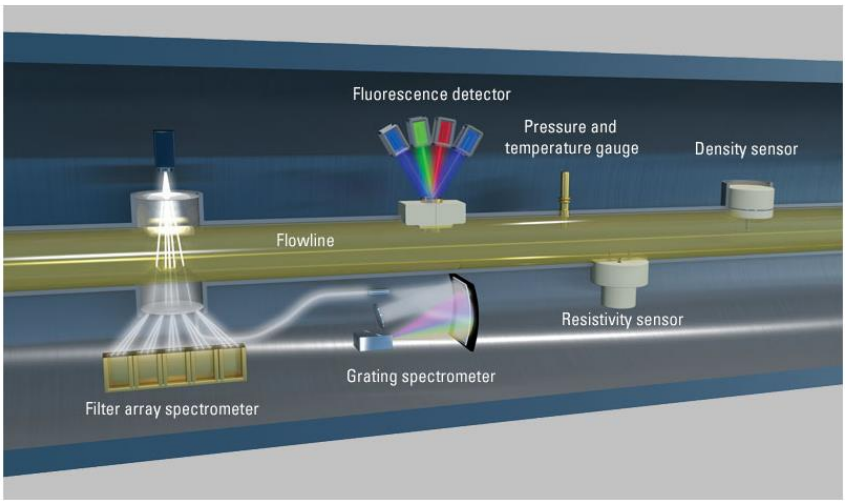

Figure 5. A schematic of the IFA which has two visible-near-infrared spectrometers using both filters and a grating, a fluorescence cell, a resistivity cell a density cell, a viscosity cell (not shown) and pressure and temperature gauges.

GC×GC and GC×GC-MS.

Gas chromatography (GC) is a powerful tool that facilitates the separation of complex molecular mixtures for compound identification and quantification. Conventional GC uses a single capillary column coated with a stationary phase that influences how compounds are separated by a single property such as molecular weight, volatility, polarity, or polarizability. GC has been very useful for analyzing complex mixtures, such as crude oil, and for resolving individual compounds of interest. However, one major limitation in conventional GC is with "unresolved complex mixtures" (UCMs) in weathered and biodegraded oils (cf. Fig. 6). In contrast, comprehensive two-dimensional gas chromatography (GC×GC) adds a second column after the primary column with a different stationary phase to separate compounds according to two chemical attributes, for example molecular weight and polarity. GC×GC offers advantages over conventional GC of separating highly complex mixtures, such as crude oil into thousands of fully resolved individual compound peaks and with low variability in response factor between compounds.[Gaines et al, 2004, 2006; Nelson et al, 2006] Additionally, compound peaks in GC×GC are less affected by coeluting components due to higher peak capacity and increased resolving power. Chemical

retention maps are generated with GC×GC, which can analyze and unravel compositional alteration of crude oils from a variety of process such as biodegradation, water washing, and thermal maturity variations.

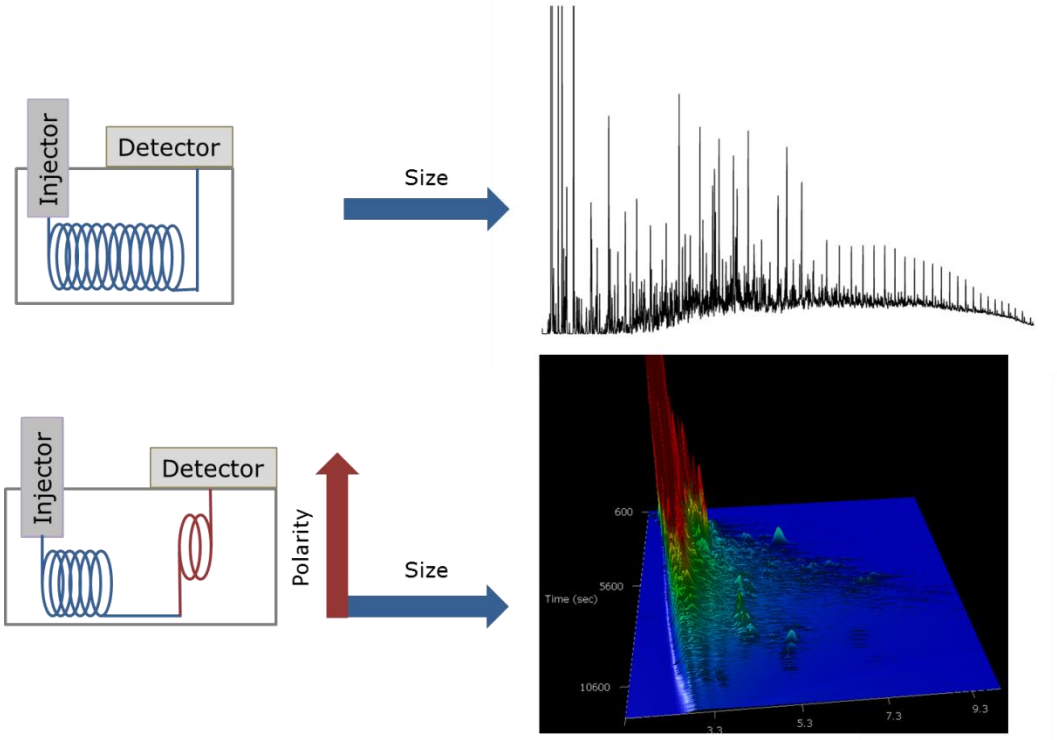

Figure 6. Comparison of conventional gas chromatography (GC) and comprehensive two-dimensional gas chromatography (GC×GC) used for data acquisition.

Conventional GC-FID was performed with an Agilent 7680 gas chromatograph equipped with a split/splitless auto-injector (7683B series) and a flame ionization detector (FID) (Agilent, Palo Alto, CA). The GC was fitted with a 20 m x 0.18 mm ID fused silica capillary column coated with a 0.4 μm thick film of 100% dimethylpolysiloxane (Rtx-1, Restek, Bellefonte, PA). Ultra high purity He was used as a carrier gas with a constant flow rate of 0.8 mL min^{-1}. Samples were injected at 300 °C with a split ratio of 25:1 with a HP 6890 series autosampler (Agilent, Palo Alto, CA). The GC oven was programmed from 35 to 335 °C at 2 °C min^{-1} with a final hold time of 10 min. Data from the FID was collected at 100 Hz and reference standards were used to identify peaks.

Two Leco Pegasus 4D GC×GC systems were used in this study, one coupled with a FID and another with a time-of flight mass spectrometer (TOFMS) (Leco, St. Joseph, MI). Each instrument was equipped with an Agilent Model 7890 GC (FID) and an Agilent Model 6890 N GC-TOFMS (time of flight mass spectrometer) (Agilent, Palo Alto, CA). Both were configured with split/splitless autoinjectors (7683B series) and dual-stage cryogenic modulators (Leco, St. Joseph, MI). The modulator operates with a cold gas jet consisting of dry N_2 cooled with liquid N_2 and a dry air hot

gas jet operated at 20 °C above the temperature of the main oven. Two capillary GC columns were connected with Press-Tight connectors (Restek, Bellefonte, PA) and were fitted in each GC×GC instrument. The first dimension (^{1}D) column was a nonpolar Rxi-1 MS (30 m × 0.25 mm ID, 0.25 µm film thickness (FID) and 60 m x 0.25 mm ID, 0.25 μm film thickness (TOFMS)) (Restek, Bellefonte, PA) and the second dimension (2D) column was a BPX-50 midpolar 50% phenyl polysilphenylene-siloxane column (1.0 m × 0.10 mm ID, 0.1 μm film thickness) (SGE Scientific, Austin, TX).

For GC×GC-FID analysis, 1 μL of each sample solution was injected into a 300 °C splitless injector with a purge time of 1.0 min. Each component of the system, the ^{1}D column, the ^{2}D column, and the dual-stage cryogenic modulator maintain individual heating controls, allowing for independent temperature operation of each element. Ultra-high purity helium was used as the carrier gas and was maintained at a constant flow rate of 1.50 mL min^{-1}. The temperature program of the main oven started isothermal at 40 °C for 1 min and then was ramped to 335 °C at a rate of 1.5 °C min^{-1}. The modulation period was 10.0 sec with a hot jet pulse at 2.5 s and a cold period of 2.5 s between stages. The ^{2}D oven was maintained at a temperature + 10 °C above the main oven. The FID signal was sampled at 100 Hz.

For GC×GC-MS, 2 μL of each sample solution was injected into a 300 °C splitless injector with a purge time of 1.0 min. Hydrogen was used as the carrier gas and was maintained at a constant flow rate of 1.00 mL min^{-1}. The temperature program started isothermal at 45 °C for 10 min than was ramped to 335 °C at a rate of 2.00 °C min^{-1}. The modulation period was 7.5 s with a hot jet pulse of 1.0 s and a cold period of 2.75 s between stages. The ^{2}D oven was maintained at a temperature +5 °C above the main oven. The transfer line from the ^{2}D oven to the TOFMS was a 0.5 m × 0.18 mm ID length of deactivated fused silica held at a constant temperature of 315 °C. The TOF detector voltage was 1335 V, and the source temperature was 220 °C. The mass spectrometer uses an electron ionization of 70 eV and operates at a push pulse rate of 50 kHz, allowing sufficient signal averaging time to ensure good signal-to-noise ratios while operating at high data acquisition rates to accurately process spectra from peaks eluting from the ^{2}D column with peak widths between 50 ms and 200 ms.

GC×GC-FID and GC×GC-MS data acquisition and processing were performed with ChromaTOF software, version 4.50 (Leco, St. Joseph, MI). Individual peaks were automatically detected on the basis of signal/noise (S/N) ratio of 100:1. Compounds were identified through reference standards, retention time, elution order, and mass spectral fragmentation patterns. Typically, the first- and second-dimension retention times are sufficient to identify the chemical class of an analyte. Further clarification of compound identifies were made by comparison against elution patterns of 12-component hopane/sterane calibration mixes (Chiron, Trondheim, Norway), other various component reference standards, or by matching component fragmentation patterns against the NIST library. After peak identification, quantification of individual components was performed by integrating the area under the FID peak.

3. Results and Discussion

Field Map.

For the reservoirs shown in Figure 7, there is a general trend for reservoirs to be deeper in the northeast and shallower in the southwest. It is thought that the source rock for the oil in these reservoirs is deeper and further to the Northeast. The process of how the crude oil filled these various reservoirs is very important in order to understand the compositional variation of oil in these different reservoirs. One possibility is that the crude oil first entered the deepest reservoir in the Northeast. This reservoir was then overfilled and the overflow oil then filled consecutively shallower reservoirs. This is called a spill-fill sequence in reservoir filling as shown schematically in Fig. 8.

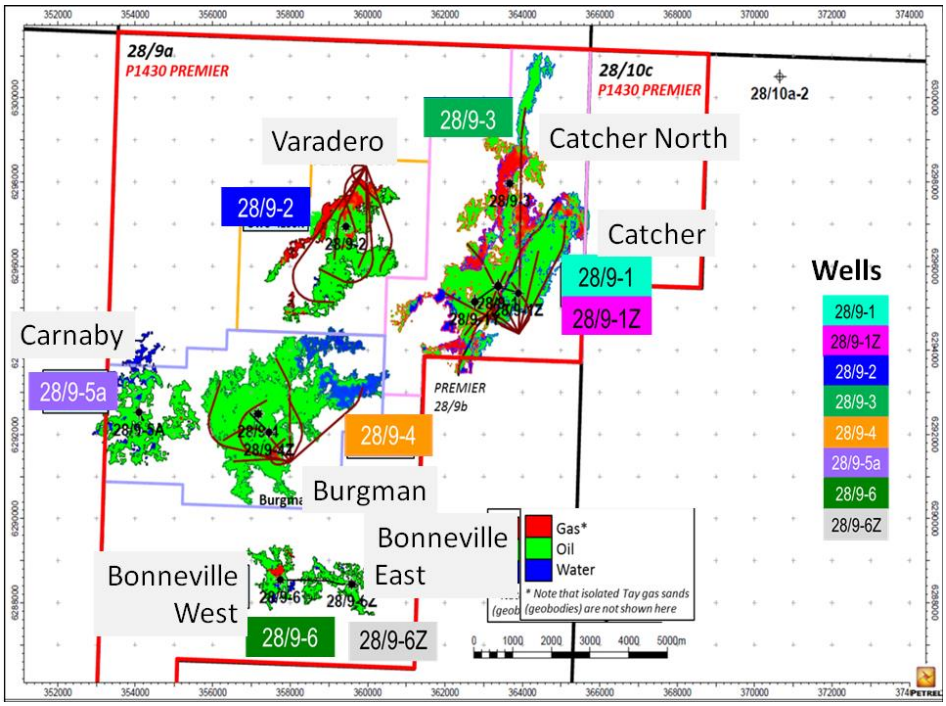

Figure 7. Field map of the Catcher Area showing the location of the eight wells examined.

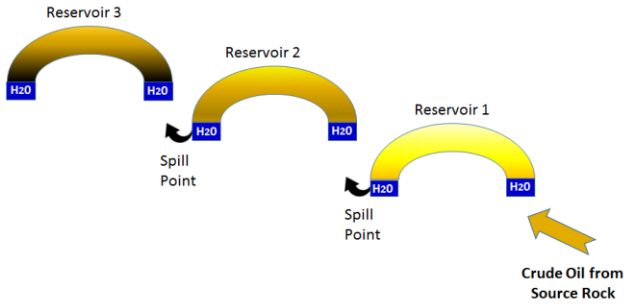

Figure 8. A 'spill-fill' sequence of three reservoirs is shown. The crude oil migrates up from a source rock deeper than the reservoirs. Here, the deepest reservoir, Reservoir 1, fills first. A common occurrence is that the reservoir overfills. Excess oil spills out of Reservoir 1 at its spill point. This oil then migrates to Reservoir 2. If a density gradient exists in Reservoir 1, as indicated by the color gradient, then the oil of greatest density spills out at the base of the oil column. This same overfilling and spilling process results in higher density oil from Reservoir 2 to spill into Reservoir 3, leaving lower density oils in Reservoir 2 and in Reservoir 1.

Asphaltene Distribution.

An important component of the spill-fill sequence depicted in Figure 8 is that the densest oil will be the first to spill out of an overfilled reservoir. This is due to the typical process of a normal reservoir charging sequence with the least mature, most dense oil emerging from the source rock first.(Tissot & Welte, 1978) As time progresses, the source rock experiences deeper burial and is exposed to higher temperatures for longer periods of time, generating lower density crude oils with higher thermal maturity levels that enter the reservoir at a later time. The highest thermal maturity and lightest oils would be the last to enter the deepest reservoirs and would not be observed in the shallower reservoirs. If the reservoirs conform to the spill-fill process, the asphaltene content of the oils will follow the overall thermal maturity and oil density content previously discussed. Greater asphaltene content implies greater oil density. Moreover, generally within individual reservoirs, there is greater asphaltene content toward the base of the oil column.(Mullins, 2008) Asphaltene content in oil is proportional to the color of the oil.[Ruiz-Morales et al, 2007; Kharrat et al, 2013] Figure 9 shows the overall asphaltene content for the crude oils in the different reservoirs described here.

The asphaltene gradient curves in Figure 9 correspond to the Flory-Huggins-Zuo Equation of State (EoS) using 2 nm asphaltene nanoaggregates from the Yen-Mullins model. The slope of the gradients increase (become less vertical) as the asphaltene content increases. The curves in Figure 9 also reflect the expectation of greater oil density via higher asphaltene content lower in the oil column for an individual reservoir. Interestingly, the overall increase in asphaltene content from the deepest to the shallowest reservoir is a factor of 3. This change in asphaltene content corresponds to a change of a factor of ten in viscosity, from ~2.1 centipoise for the deepest oils to ~25 centipoise for the shallowest oils. Of course, the colder temperatures of the shallower reservoirs yields an increase in viscosity of the contained oils. Additionally, the 3x increase in asphaltene content is the same increase observed in the fluid gradients in the

Bhagyam reservoir (cf Fig. 1) where the oils have biodegradation levels ranging from 0 to 6 on the Peters-Moldowan scale. Thus, the extent of biodegradation must be evaluated in these oils and it remains important to elucidate the primary factors that govern oil quality in these reservoirs.

If active biodegradation is occurring in the reservoir, then the most biodegraded oil will also spill out of the lower reservoirs, as the process of biodegradation selectively removes lighter components while concentrating heavier components. The location of the most biodegraded oil is at the base of the reservoir at the oil-water contact, as biodegradation requires appropriate temperatures, nutrients, and a source of water for oil-consuming microflora to flourish.(Head et al, 2003) Figure 10 shows conventional GC chromatograms from the oils in the Catcher Area oilfield. Generally the deeper samples have a greater fraction of *n*-alkanes and other alkanes (which appear as narrow spikes) consistent with the concept of variable biodegradation in the field largely dependent on reservoir depth. In addition, the filtrate from the oil-based mud drilling fluid is evident.

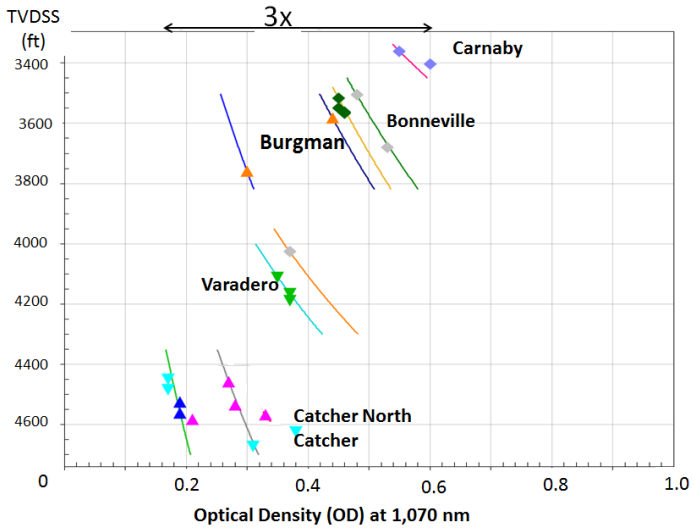

Figure 9. The DFA-measured color (optical density) of the crude oils at a wavelength of 1070 nm (after baseline subtraction). Oil color is proportional to asphaltene content. The deeper reservoirs have lower concentrations of asphaltenes, consistent with the spill-fill sequence of reservoir filling with lighter oils in deeper reservoirs and heavier oils in shallower reservoirs. Within individual reservoirs, there is generally greater asphaltene content towards the base as expected.

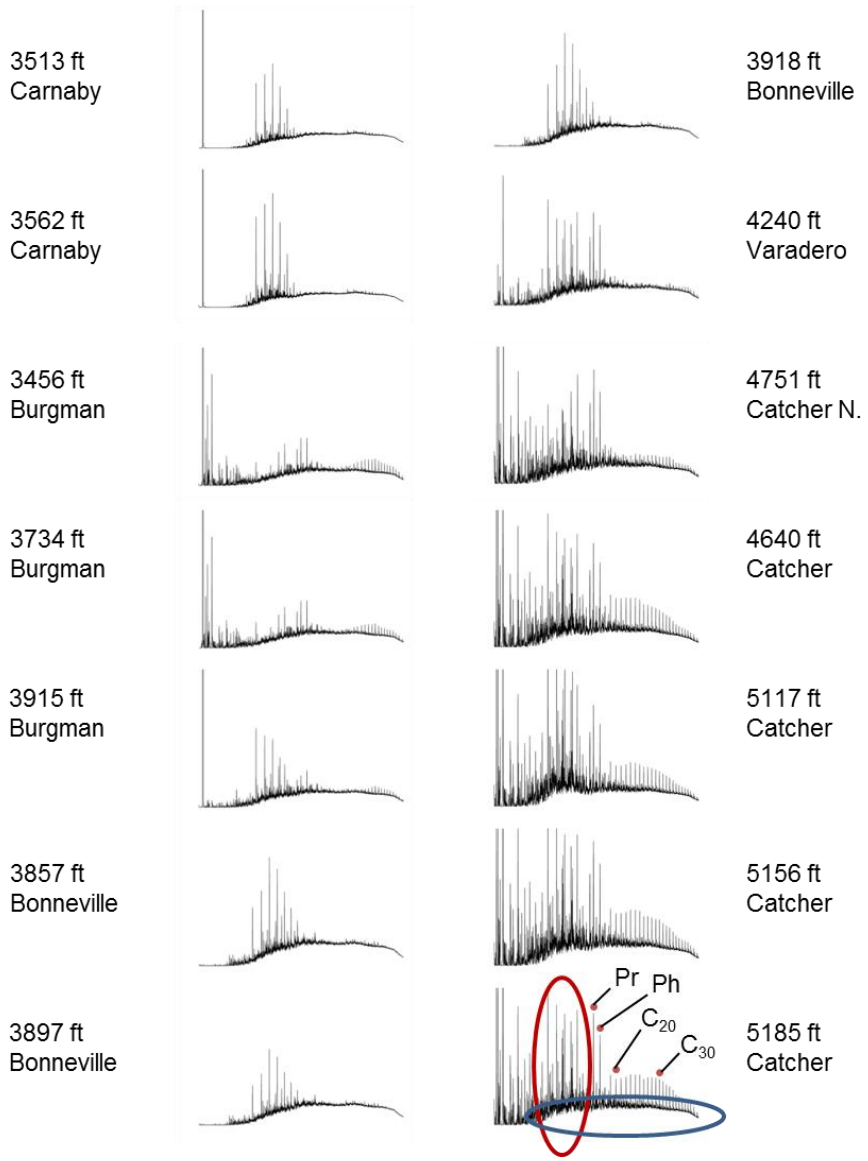

Figure 10. Conventional whole oil gas chromatograms of crude oil samples from all reservoirs studied. Pristane (Pr), phytane (Ph), and n-alkanes (C_{20}, and C_{30}) are marked with red dots. The circled region in red is where drilling mud filtrate contamination appears. The circled region in blue is the location of the unresolved complex mass (UCM). Biodegradation results in a decrease in the n-alkane and other alkane peaks and a relative increase in UCM height. Shallower reservoirs are seen to be more biodegraded than deeper reservoirs.

Crude Oil Compositional Analysis.

Reservoir temperatures for this field range between 40 °C in shallower reservoirs to 60 °C for deeper reservoirs. With these temperatures and availability of water, it is expected that the reservoirs are undergoing active biodegradation. Water washing especially enhanced by biodegradation can also occur. In addition, the crude oils in these reservoirs can have different levels of thermal maturities associated with their origins. Finally, in the process of drilling wells

in this oil field, oil-based mud was used. These drilling fluids consist of a base oil with high concentration of *n*-alkanes in the range of 10 to 14 carbons. All of these complexities need to be resolved and a preferred method is use of GCxGC. Figure 11 indicates how these different factors that influence oil composition separate in the GCxGC chromatogram.

Filtrate from oil based mud (OBM) drilling fluid contamination is present in all samples, appearing as large peaks in the C_{10} to C_{14} region of chromatograms (cf. Figure 11); this range is avoided in analysis to avoid misinterpretation. Figure 11 shows the different chemical classes that are useful for corresponding analyses. Biodegradation for these crude oils can be analyzed using alkanes outside the contamination range and using the biomarkers. Water washing can be analyzed using the naphthalenes and other multi-ring aromatics. Thermal maturity can be analyzed using the biomarker range. Figure 12 shows an expanded view of a GCxGC chromatogram showing the chemical specificity that is very useful for quantitative analyses, for example, emphasizing the n-alkanes along with pristine and phytane that are useful for analyzing biodegradation. In addition, naphthalene and alkylnaphthalenes are shown which are particularly useful for analysis of water washing due to varying degrees of water solubility.

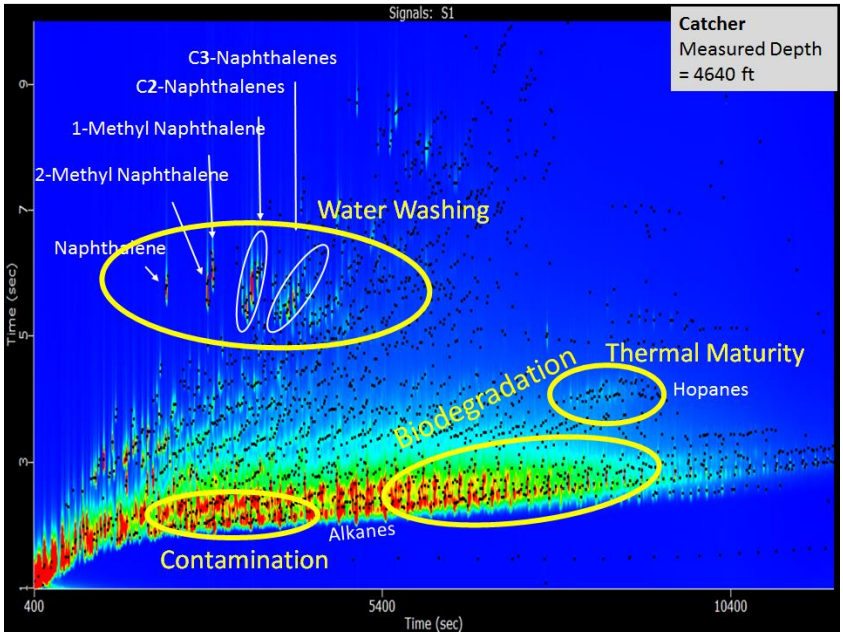

Figure 11. Comprehensive two-dimensional gas chromatography (GCxGC) with flame ionization detection (FID) for a sample from the deepest reservoir Catcher at a measured depth 4640 feet. Compounds separate out according to different chemical classes. Contamination from the OBM drilling fluid is largely isolated as indicated [Reddy et al, 2007] and this region is not considered for analysis of the crude oil samples. Water washing can be analyzed using water soluble compounds, such as naphthalenes while biodegradation impacts the n-alkanes first before moving onto branched molecules, aromatics and biomarkers. Thermal maturity of the samples is assigned through the biomarkers, specifically hopanes and steranes.

Biodegradation.

Examination of these samples with GCxGC allows the Peters-Moldowan rank of biodegradation to be determined. Figure 12 shows peaks for n-alkanes with 16, 17 and 18 carbons. In addition, pristine and phytane are shown. For the ratios pristine/n-C_{17} and phytane/n-C_{18} of about 1/10, the Peters-Moldowan rank of biodegradation is about 2.[Peters et al, 2005]

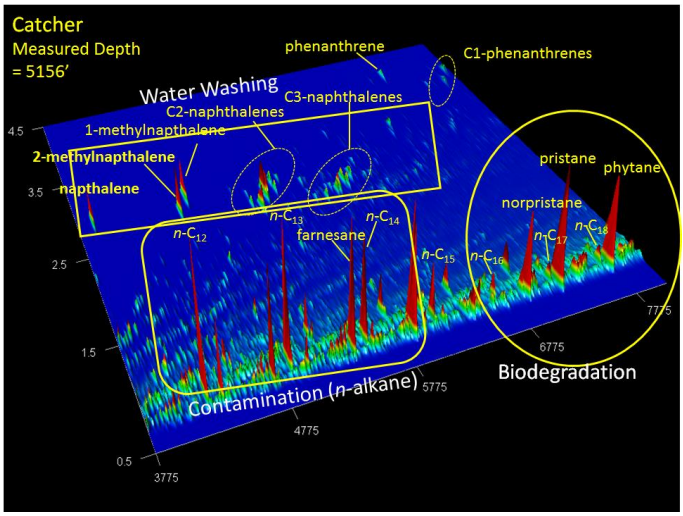

Figure 12. An expanded region of the GC×GC chromatogram for a Catcher reservoir crude oil. The large ratios of pristane (Pr) to n-C_{17} and phytane (Ph) to n-C_{18} indicate mild biodegradation levels of 2 on the Peters-Moldowan scale. The large n-alkane peaks for n-C_{12}, n-C_{13}, and n-C_{14} and to a lesser extent n-C15 are contamination from oil-based drilling mud filtrate (OBM).

More extensive loss of n-alkanes and isoalkanes indicates a greater extent of biodegradation. Figure 13 shows three oils of very different scales of biodegradation as determined by successively increasing loss of alkanes. As discussed above the Catcher oil has a rank of PM~2. The more extensive loss of both *n*-alkanes and isoalkanes corresponds to a rank of PM~4. The loss of alkanes is sufficiently severe for the Carnaby sample that it is preferred to use the biomarker range of the GCxGC chromatogram for quantification of the extent of biodegradation. In Figure 13 as in Figure 12, a variable magnitude of *n*-alkanes peaks from the drilling fluid filtrate are evident for *n*-C_{12} through *n*-C_{14} and to a lesser extent for *n*-C_{15}.

A) Catcher
M. D. = 5160 ft
PM = 2

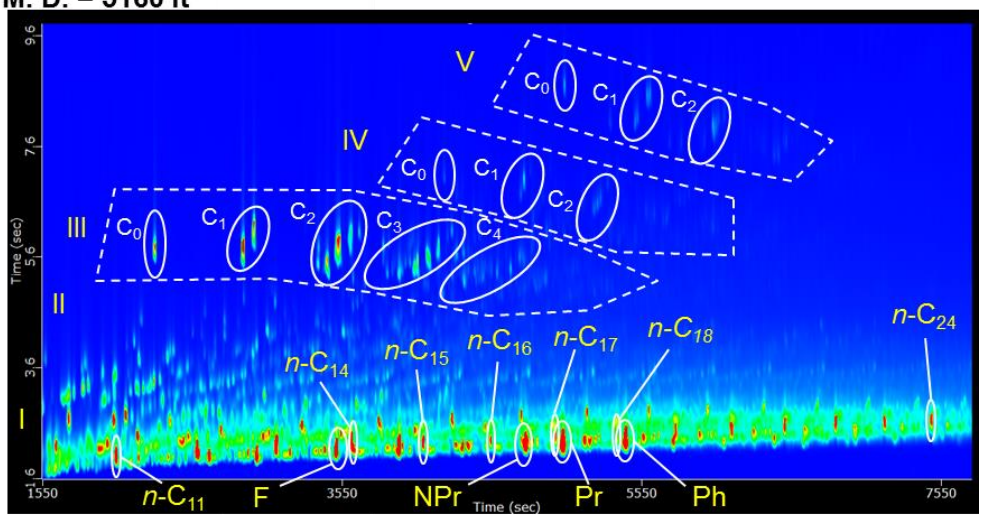

B) Burgman
M. D. = 3734 ft
PM = 4

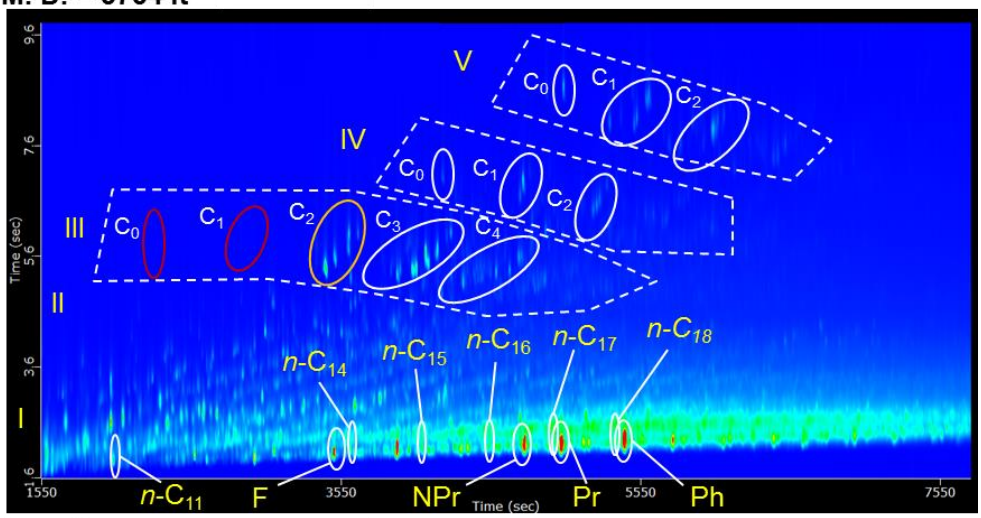

C) Carnaby
M. D. = 3513 ft
PM = 6+

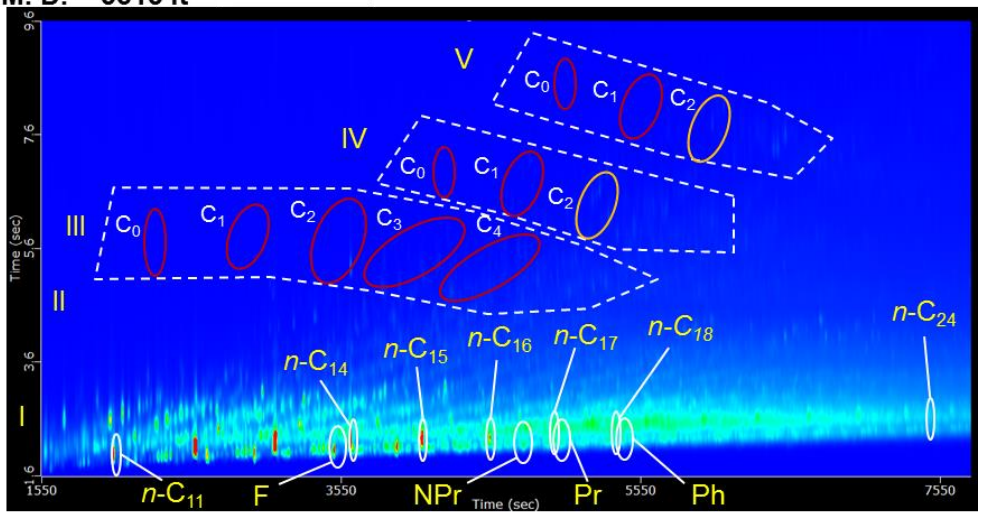

Figure 13. GC×GC chromatograms showing the n-alkane (C_9-C_{21}) line and aromatics (1-3 ring) for crude oils from three reservoirs, A) Catcher, B) Burgman, and C) Carnaby. The oils have distinctly different levels of biodegradation as indicated by the different n-alkane and isoalkane content. The Catcher sample has small n-alkane peaks and large isoalkane peaks such as pristine (Pr) and phytane (Ph). The Burgman sample has lost the n-alkanes but retains isoalkanes. The Carnaby sample has neither n-alkanes nor isoalkanes except for those from the mud filtrate. Water washing is evident in the aromatics and is discussed below. Major groups: I = Alkyl benzenes, II= Indenes, III = naphthalenes, IV = fluorenes, V = phenanthrenes and dibenzothiophenes. C_1, C_2, C_3, and C_4 in the naphthalene and phenanthrene groups indicate the degree of methylation of the structure. For example, C_2 is two methyl groups or one ethyl group.

Figure 14 shows the biomarker region for three crude oils. For all samples analyzed (many not shown), the only crude oil sample that differed in the biomarker region is the Carnaby sample. Figure 15 shows that the Carnaby sample had additional peaks that indicate the appearance of 25-norhopanes that are not present in other any other samples. 25-norhopanes result from microbial demethylation of hopanes during the biodegradation process [Peters et al, 1996]. This process corresponds to a biodegradation rank of PM 6 indicating severe biodegradation and alteration of different chemical components..

A) Catcher
M. D. = 5160 ft

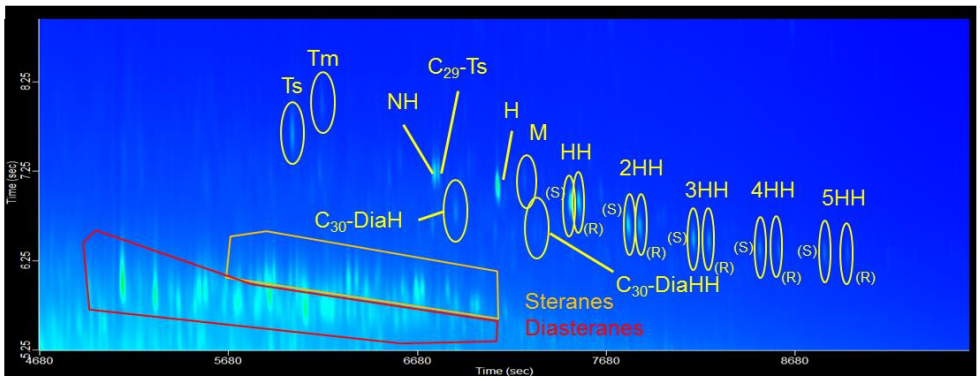

B) Burgman
M. D. = 3734 ft

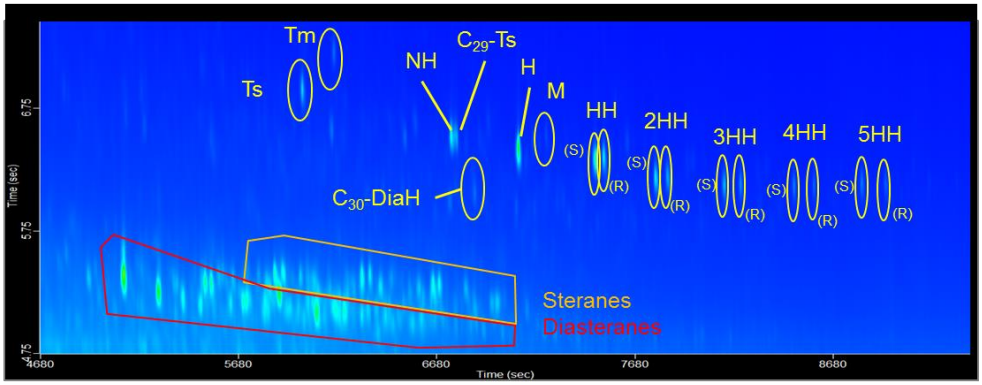

C) Carnaby
M. D. = 3513 ft

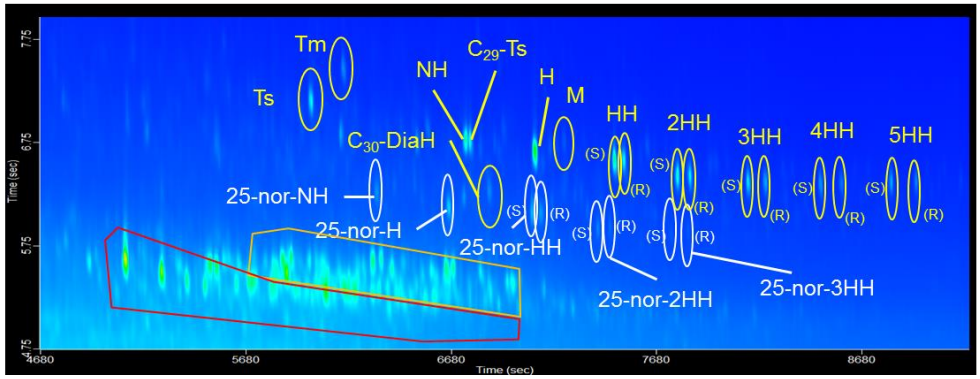

Figure 14. The hopane, sterane, and diasterane biomarker region for crude oils from three reservoirs, Catcher, Burgman, and Carnaby. All crude oils except Carnaby have a similar appearance of the hopane region. For Carnaby, eight peaks attributed to 25-norhopanes (marked in white) appear below the hopane series, indicating that the Carnaby oils are heavily biodegraded (PM 6). 25-norhopanes were not detected in any other samples.

To confirm the identity of these new peaks as 25-norhopanes, GCxGC-MS (time-of-flight mass spectrometry) was performed. With normal hopanes, a combination of *m/z* of 191 and peak position in the two-dimensional chromatogram is used to confirm peak identities. In Figure 15,

the *m/z* 191 scan is shown in the top left panel, confirming locations of a variety of hopane compounds. However, there is a series of peaks near the C_{30}-diahopane series that indicate the presence of possible 25-norhopanes. To detect the presence of 25-norhopanes, which are biodegraded hopanes via methyl removal [Peters et al, 2005] a diagnostic scan of *m/z* 177 is used, as shown in the lower chromatogram in Figure 15. The fragmentation patterns in Figure 25 (two right panels) shows the first two 25-norhopanes in the series, 25-nor-norhopane (25-nor-NH) and 25-norhopane (25-nor-H). Presence of this 25-norhopane series in Carnaby supports the assignment of PM 6 in these samples.

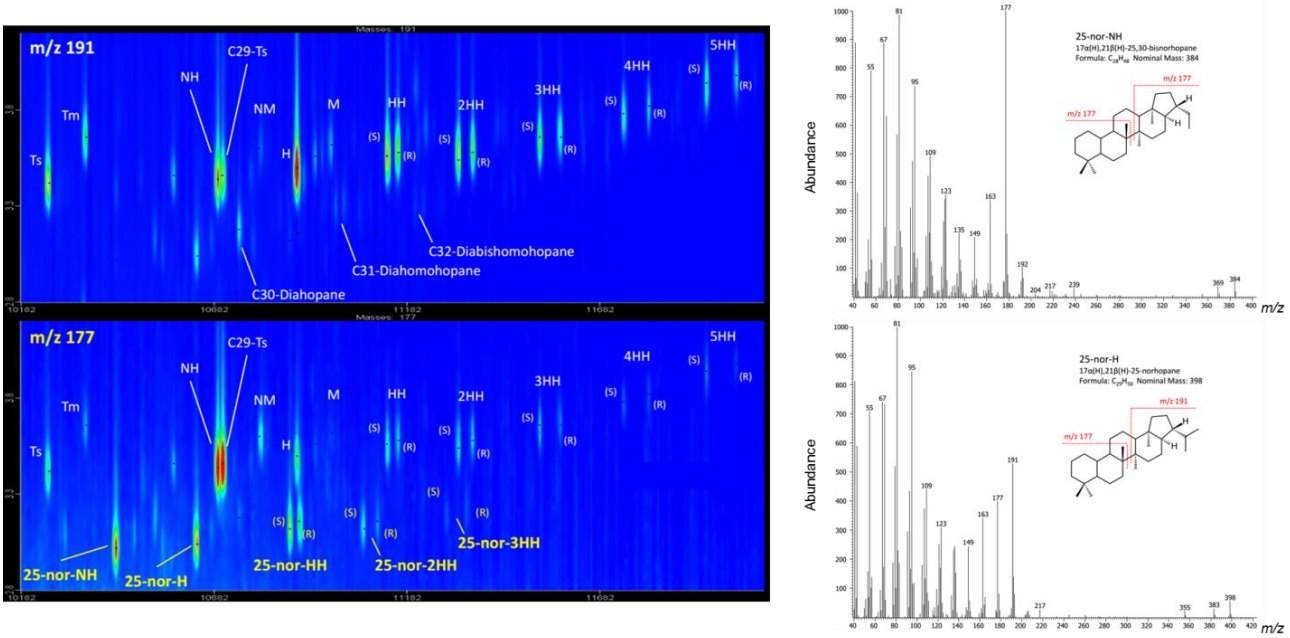

Figure 15. GC×GC-MS of the hopane series of the biomarker region. Left images: diagnostic scans of m/z 191 and 177 for hopanes and 25-norhopanes respectively reflecting replacement of –CH_3 by –H. Right: Mass spectrometry fragmentation patterns for two specific 25-norhopanes, 25-nor-NH and 25-nor-H, as labeled in the figure. The fragmentation patterns are characteristic validating the assignments for 25-norhopanes and confirm biodegradation levels of PM 6 in the Carnaby reservoir. 25-norhopanes were not observed in any of the other reservoirs.

Table 1 presents the rank of biodegradation using the Peters-Moldowan scale of all samples analyzed. The samples are listed shallowest to deepest. There is a clear trend of a greater extent of biodegradation for reservoirs at shallower depth. This is consistent with the spill-fill sequence for reservoir filling schematically shown in Fig. 8. The most biodegraded oils in a reservoir are at the oil-water contact [Head et al, 2003, Zuo et al, 2015] which is where the oils spill out of the reservoir.

Table 1. The biodegradation rank on the Peters-Moldowan scale for the oils in this study for the various reservoirs at different measured depths. The oils span a large range in biodegradation and the values are consistent with a spill-fill scenario for reservoir filling with the most biodegraded

oils in the shallowest reservoirs.

Depth (ft)	Field	PM (1993) Rank
3513	Carnaby	6
3562	Carnaby	6
3734	Burgman	4
3756	Burgman	4
3857	Bonneville	4-5
3897	Bonneville	4-5
3915	Bugman	4
3918	Bonneville	5
4240	Varadero	2-3
4640	Catcher	2
4751	Catcher North	2
5117	Catcher	2
5156	Catcher	2
5185	Catcher	2

Water washing.

Figure 13 shows a successively increasing loss of water soluble alkylnaphthalenes in the different samples. Figure 16 shows a comparison of two-ring aromatics and 3-ring aromatics for three different samples. There is a dramatic, systematic change in chemical components of these samples. In particular, the more water soluble components are found to be selectively removed. For aromatic compounds, water solubility decreases with increasing alkyl substitution and with increasing numbers of fused rings. Figure 16 shows that the disappearance of these light aromatics is in order of their water solubility. For example, the Catcher sample (Fig. 15A) contains naphthalene, the 1- and 2-methylnaphthalene while the Burgman sample (Fig. 15B) is lacking these components. In addition, the Burgman sample also lacks some of the naphthalenes with two alkyl carbon substituents. Nevertheless, Fig. 16 shows the three-ring aromatics in Catcher and Burgman are very similar in accord with their lower solubility.

The Carnaby sample is lacking virtually all of the alkylnaphthalenes, the three ring aromatics without alkyl substitution and the methylated three ring aromatics. Nevertheless, the Carnaby sample has the same complement of phenanthrenes with three methyl substitution as do the Catcher and Burgman samples. Thus, the Carnaby sample exhibits a greater degree of water washing than the Burgman sample.

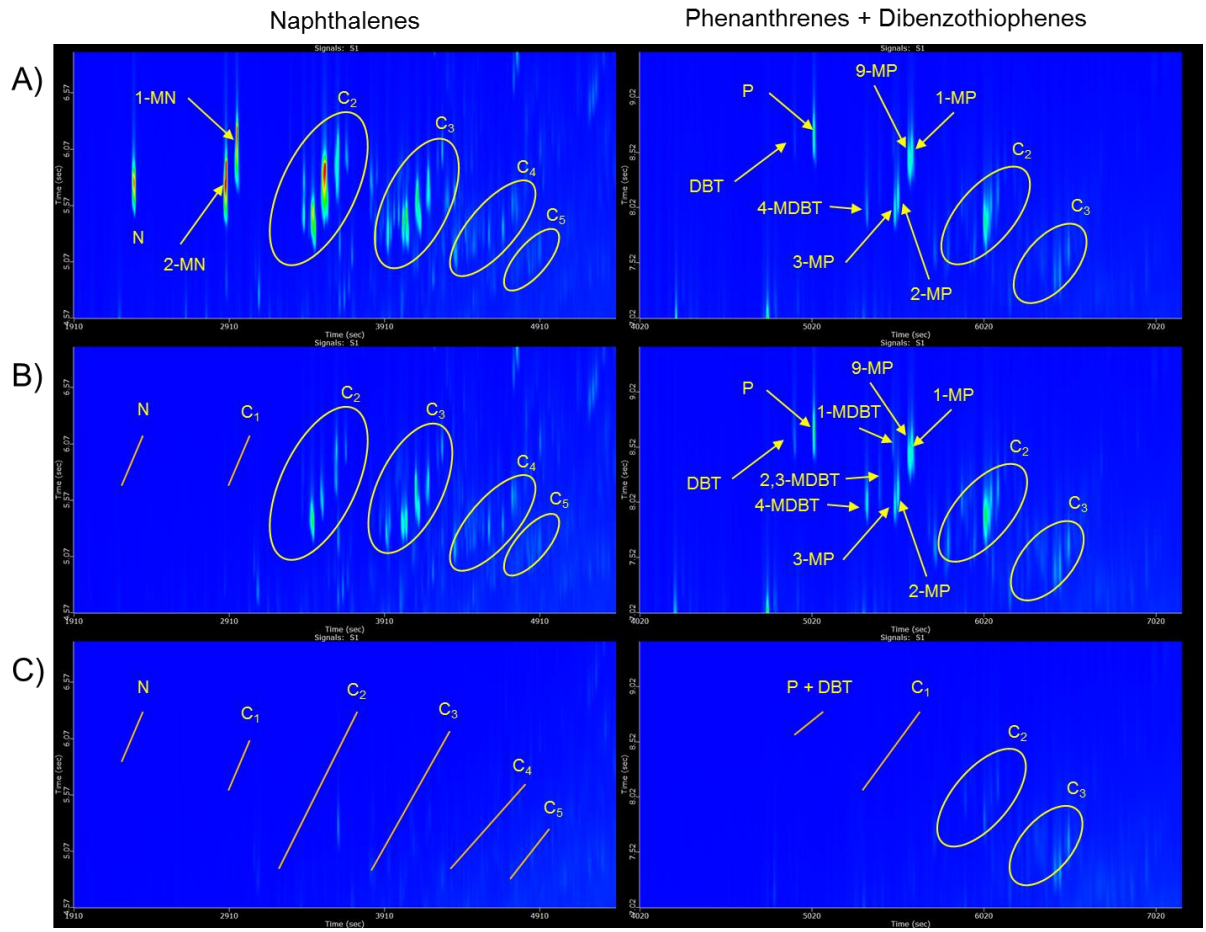

Figure 16. Naphthalenes (left) and phenanthrenes and dibenzothiophenes (DBT) (right) from A) Catcher, B) Burgman, and C) Carnaby reservoirs. The progression of removal of compounds from a combination of water washing and biodegradation can be observed. Naphthalene and alkylated naphthalenes will be the first compound to be removed according to degree of alkylation while phenathrene, dibenzothiophene and alkylated versions remain unaltered until the biodegradation level reaches PM 6 in Carnaby. Circled peaks indicate present/detected peaks while lines mark the region of the chromatogram where the peaks would normally appear. N = naphthalene, 1-MN = 1-methylnaphthalene, 2-MN = 2-methylnaphthalene DBT = dibenzothiophene, P = phenanthrene, k-MDBT = methyldibenzothiophene where k refers to the position of the methyl substitution, and k-MP = methylphenanthrene where k refers to the position of the methyl substitution. C_1, C_2, and C_3 = methyl, two alkyl carbon, and three alkyl carbon additions to naphthalene and phenanthrene and dibenzothiophene rings.

As noted, aromatic compounds are decreasingly water soluble with increasing alkyl substitution and with increasing numbers of fused rings. Table 2 validates these generalities

Table 2. Solubility of selected aromatic compounds in water.[Schwarz, 1977]

Compound	Solubility (mg/L)
Benzene	1800
Toluene	520
Naphthalene	32
1-methylnaphthalene	25
2-methylnaphthalene	26
1-ethylnaphthalene	8
Anthracene	0.04
Phenanthrene	0.9
Dibenzothiophene	1.5
Pyrene	0.09
Benzo[e]pyrene	0.005

The extent of water washing in these oils might be considered surprising in that crude oils from the Llanos basin exhibit much lesser extents of water washing in spite of the much greater aquifer replenishment in the Llanos basin. The surface waters of the Llanos basin form the Amazon river, by far the largest river in volumetric flow on the planet. Fig. 3 shows that one Llanos basin oil lacks only naphthalene. The origin of the contrast in water washing is due to the active biodegradation in the Catcher Area reservoirs, while the Llanos basin reservoirs are currently at high temperatures beyond those of biodegradation. Consequently, water soluble components that partition into the aquifer can be/ are consumed by biodegradation in the Catcher Area reservoirs precluding any flux of these components from the aquifer to the oil. In contrast, in the Llanos Basin reservoirs, water washing requires the water soluble components to be transported by diffusion or convection away from the oil-water contact to enable a continued flux of water soluble components out of the crude oil. Both diffusion and aquifer convection are quite slow in geologic time.[Zuo et al, 2015] Biodegradation assisted water washing is taking place. Further validation of this concept is obtained by comparing general chemical tendencies of water solubility versus biodegradation.

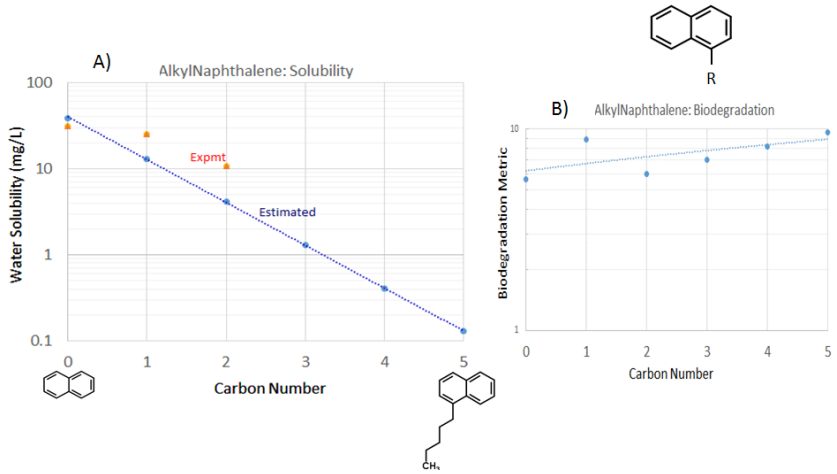

Figure 17. The left, A), shows estimation of dependence of water solubility in mg/L of naphthalene and alkylnaphthalenes on the extent of alkylation. B) shows an estimate of susceptibilities to biodegradation of the naphthalenes. [ChemSpider]

Figure 17 indicates that it is the variable water solubility, not the biodegradation that accounts for the losses of various naphthalenes observed in Figure 16.[ChemSpider] There is a large dependence of water solubility of naphthalene on the extent of alkylation, whereas the is little variation of biodegradation on alkylation of the naphthalenes. Consequently, the observed loss of alkylated naphthalenes is consistent with water washing. Biodegradation enhances the water washing. Once a naphthalene molecule dissolves in water, it is consumed by microbes thereby facilitating more flux of naphthalene molecules into the aqueous phase. In the Llanos basin example in Figure 3, the oilfield temperature of 105°C is too hot for biodegradation. Consequently, naphthalenes that dissolve in water must be transported away from the oil-water contact by diffusion or convection in order for the flux of naphthalenes to continue from oil to water. In the Catcher Area Reservoirs, Figure 12 shows biodegradation-enhanced water solubility.

Thermal Maturity Markers.

In a normal spill-fill sequence, less thermally mature crude oils are the first to enter the reservoir (e.g. Reservoir 1 in Figure 8). Over time, more thermally mature oils will continue to fill and eventually overfill the reservoir. The less thermally mature oils are more dense and will spill out of the deepest reservoir and enter the next shallowest reservoir (e.g. Reservoir 2 in Figure 8). Consequently, analysis of thermal maturity markers should vary systematically, with low thermal maturity oils in shallower reservoirs while higher thermal maturity oils should be in the deeper reservoirs. Figure 18 shows a combination of four thermal maturity biomarkers, each showing

expected overall thermal maturity trends in the oils: higher thermal maturity oils deeper in the reservoir and lower thermal maturity oils shallower in the reservoir. Generally, the thermal maturity markers compare ratios of more stable to less stable stereoisomers of a given compound. With increasing temperature thus maturity, the more stable form becomes more predominant. Analysis of thermal maturity markers for maturity estimation is routine. Nevertheless, there can be other influences than maturity on these evaluations. For example, the compounds Ts and Tm are acknowledged to be the best for thermal maturity analysis [Peters et al, 2005], however, difference source inputs can impact Ts and Tm ratios and alter the usefulness of the ratio in unexpected ways.[Peters et al, 2005] Consequently, it is best to evaluate several thermal maturity markers for validation.

The biomarkers Ts/(Ts+Tm) in Figure 18 shows a decrease in overall thermal maturity across different reservoirs with decreasing depth. Other thermal maturity markers such as C_{29} $\beta\beta/(\alpha\alpha+\beta\beta)$, C_{30}Dia/(C_{30}Dia+H), and C_{32} 22S/(22S+22R) are used to support this overall trend. Thermal maturity differences in each individual reservoir are subtle and can reflect either small variations in organic facies in either the source rock or from within the reservoir itself. For example, in Catcher the bottom three points while relatively close, have a trend opposite to the expected fill sequence. That is, the least mature should be at the base but for these three points, the most mature is at the base. These variations are small and are evidently not reliable.

The ratio C_{32} homohopane 22S/(22S+22R) is less than the equilibrium value of 0.55 to 0.60 over the depth interval of the different reservoirs examined and increases with depth across different reservoirs, indicating lower thermal maturity oils at shallower reservoir depths. The ratio C_{30}Dia/(C_{30}Dia+H) compares the greater thermal stability of diahopane against hopane and is useful for determining oils in the late oil window level of thermal maturity. This marker also follows the same trend as the other markers, increasing in abundance with increasing thermal maturity (Cornford et al, 1988; Moldowan et al, 1991) with an equilibrium cut-off of 0.45.

The ratio C_{29} $\beta\beta/(\alpha\alpha+\beta\beta)$, in addition to evaluating thermal maturity, can reflect $\beta\beta$ enrichment during migration (Seifert et al, 1980; Davies, 1997). This would be reflected in C_{29} $\beta\beta/(\alpha\alpha+\beta\beta)$ showing an opposite trend to the expected thermal maturity values that the other markers note. No enrichment is observed in these reservoirs due to the spill-fill nature of charging rather than migrated oils entering the reservoir. In C_{29} $\beta\beta/(\alpha\alpha+\beta\beta)$, the same trend of more thermally mature oils deeper and less thermally mature oils shallower in the reservoir is observed.

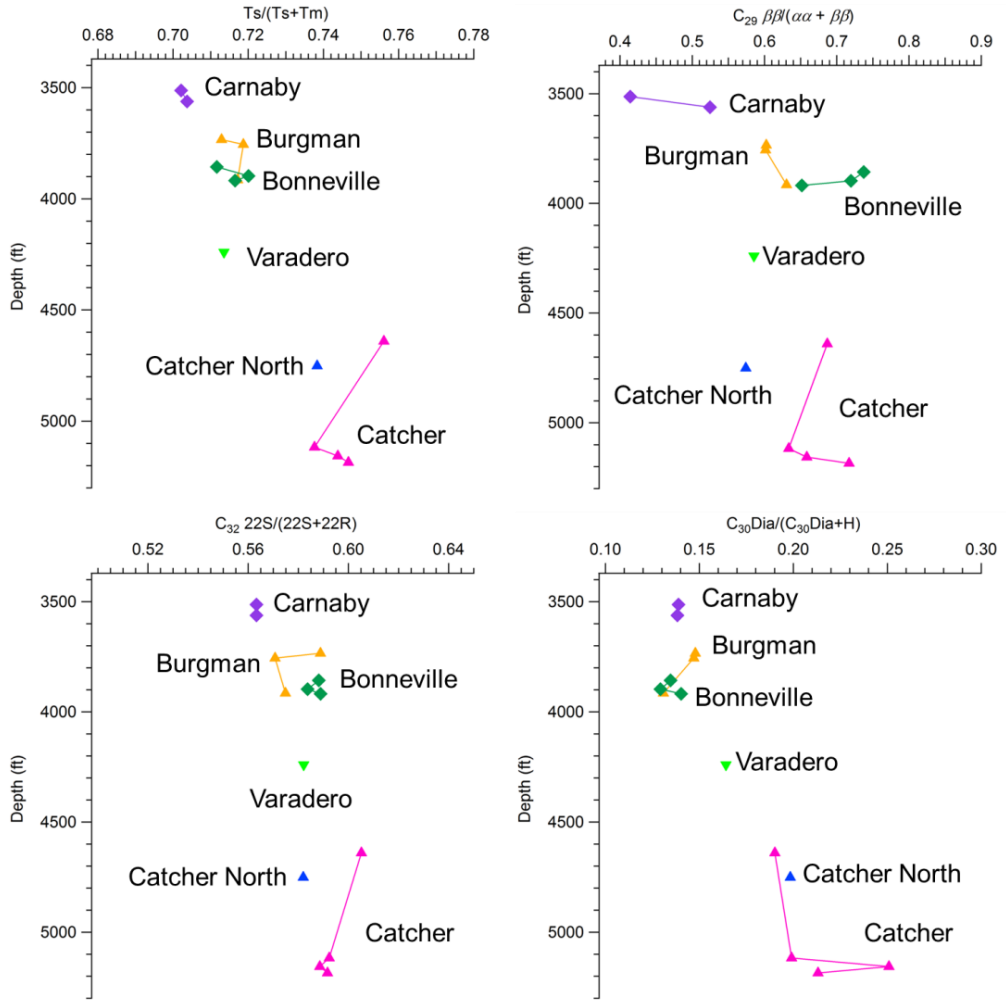

Figure 18. Ts/(Ts+Tm), C_{29} ββ(αα+ββ), C_{32} 22S/(22S+22R), and C_{30}Dia/(C_{30}Dia+H) ratios all showing the expected thermal maturity variation for a spill-fill sequence for Catcher area reservoirs. Thermal maturity increases to the right for all markers presented. The most mature crude oils in the reservors are the Catcher and Catcher North oils with the least mature are the Carnaby oils. This evaluation is not affected by the levels of biodegradation observed.

Asphaltenes; and Biodegradation, Water Washing and Thermal Maturity. The asphaltene content in the Catcher Area oils show an increase of a factor of three. As shown in Fig. 1 and discussed elsewhere,[Head et al, 2003] biodegradation gives such an increase of a factor of three in going from 0 to 6 on the Peters-Moldowan scale. This is because the microbes consume approximately 2/3 of the oil over this range thereby concentrating the asphaltenes, which the microbes do not consume. However, the Catcher Area oils show a smaller variation of biodegradation of 2 to 6. Thus a smaller increase in asphaltene content than a factor of three is accounted for by the biodegradation. Water washing, which is greater for the more biodegraded oils, causes a loss of light, water soluble components; thus, water washing increases the

asphaltene content (asphaltenes are not water soluble). In addition, crude oils of lower thermal maturity generally have greater concentrations of asphaltenes. Thus, the thermal maturity variations determined for the Catcher Area oils also act to increase asphaltene content in the shallower reservoirs. These three factors, biodegradation, water washing and thermal maturity variations all act in concert to account for the factor of three variation of asphaltenes in the Catcher Area oils.

Conclusions

Downhole fluid analysis (DFA), which determines relative asphaltene content among other fluid parameters and GCxGC chromatography with geochemical interpretation create a powerful combination to address complex reservoir issues. Here, we determine the factors that influence the factor of three difference in asphaltene content which results in a factor of ten change in viscosity, of the Catcher Area oils. A spill-fill sequence of reservoir filling was tested by overall asphaltene content and by detailed chemical analyses. GCxGC enables separation of contamination from wellbore drilling fluids from other chemical metrics of interest. The extent of biodegradation was determined for these oils which ranged from 2 to 6 on the Peters-Moldowan scale. Biodegradation-enhanced water washing is also quite evident in these oils and scales with the large range in biodegradation. In addition, thermal maturity variations were checked using four different markers; nearly uniform consistency was obtained. Low maturity oils charged first followed by higher maturity oils, with the lower maturity oils spilling to shallower reservoirs. The combined DFA and GCxGC analysis enables adoption of a robust, simple description of the reservoirs.

Appendix

Abbreviation	Compound Name	Formula
Pr	Pristane	$C_{19}H_{40}$

Ph	Phytane	$C_{20}H_{42}$
N	Naphthalene(s)	
P	Phenanthrene(s)	
DBT	Dibenzothiophene(s)	
Ts	18α(H)-22, 29, 30-trinorneohopane	$C_{27}H_{46}$
Tm	17α(H)-22, 29, 30-trinorhopane	$C_{27}H_{46}$
NH	17α(H), 21β(H)-30-norhopane	$C_{29}H_{50}$
C_{30}-Dia		
C_{30}-DiaHH		
C_{30}-DiaBisHH		
NM	17β(H), 21α(H)-norhopane	$C_{29}H_{50}$
H	17α(H), 21β(H)-hopane	$C_{30}H_{52}$
M	17β(H), 21α(H)-hopane	$C_{30}H_{52}$
HH (S)	17α(H),21β(H)-22(S)-homohopane	$C_{31}H_{54}$
HH (R)	17α(H),21β(H)-22(R)-homohopane	$C_{31}H_{54}$
2HH (S)	17α(H),21β(H)-22(S)-bishomohopane	$C_{32}H_{56}$
2HH (R)	17α(H),21β(H)-22(R)-bishomohopane	$C_{32}H_{56}$
3HH (S)	17α(H),21β(H)-22(S)-trishomohopane	$C_{33}H_{58}$
3HH (R)	17α(H),21β(H)-22(R)-trishomohopane	$C_{33}H_{58}$
4HH (S)	17α(H),21β(H)-22(S)-tetrakishomohopane	$C_{34}H_{60}$
4HH (R)	17α(H),21β(H)-22(R)-tetrakishomohopane	$C_{34}H_{60}$
5HH (S)	17α(H),21β(H)-22(S)-pentakishomohopane	$C_{35}H_{62}$
5HH (R)	17α(H),21β(H)-22(R)-pentakishomohopane	$C_{35}H_{62}$
25-nor-NH		
25-nor-H		
25-nor-HH (S)		
25-nor-HH (R)		
25-nor-2HH (S)		
25-nor-2HH (R)		
25-nor-3-HH (S)		
25-nor-3-HH (R)		

Bartha, A.; De Nicolais, N.; Sharma, V.; Roy, S.K.; Srivastava, R.; Pomerantz, A.E.; Sanclemente, M.; Perez, W.; Nelson, R.K.; Reddy, C.M.; Gros, J.; Arey, J.S.; Lelijveld, J.; Dubey, S.; Tortella, D.; Hantschel, T.; Peters, K.E.; Mullins, O.C.; Combined petroleum system modeling and comprehensive two dimensional gas chromatography to improve understanding of the crude oil chemistry in the Llanos Basin, Colombia, Energy & Fuels. **2015**, 29, 8, 4755–4767

ChemSpider, Royal Society of Chemistry, http://www.chemspider.com/Default.aspx

Cornford, C.; Christie, O.; Endresen, U.; Jensen, P.; Myhr, M. B. *Org. Geochem.* **1988**, *13*, 135-143

Davies, C. P. N. *Org. Geochem.* **1997**, *27*, 537-560

Dong, C.; Petro, D.; Pomerantz, A.E.; Nelson, R.L.; Latifzai, A.S.; Nouvelle, X.; Zuo, J.Y.; Reddy, C.M.; Mullins, O.C.; New Thermodynamic Modeling of Reservoir Crude Oil, Fuel, **2014,** 117, 839-850,

Farrimond, P.; Taylor, A.; Telnæs, N. Biomarker maturity parameters: the role of generation and thermal degradation. *Org. Geochem.* **1998**, *29*, 1181-1197

Forsythe, J.; Pomerantz, A.E.; Seifert, D.J.; Wang, K.; Chen, Y.; Zyo, J.Y,; Nelson, R.K.; Christopher M. Reddy, C.M.; Schimmelmann, A.; Sauer,P.; Peters, K.E.; Mullins, O.C.; A Geological Model for the Origin of Fluid Compositional Gradients in a Large Saudi Arabian Oilfield: An Investigation by Two-Dimensional Gas Chromatography and Asphaltene Chemistry, Energy & Fuels, **2015**, 29 (9), 5666–5680

Freed, D.E.; Mullins, O.C.; Zuo, J.Y.; Asphaltene gradients in the presence of GOR gradients, Energy & Fuels, **2010**, 24 (7), 3942-3949, (2010)

Gaines, R.B., Frysinger, G.S., Temperature requirements for thermal modulation in comprehensive two-dimensional gas chromatography, J. Separation Science, **2004**, 27, 380-388

Gaines, R.B., Frysinger, G.S., Reddy, C.M., Nelson, R.K. in: Z. Wang, S. Stout (Eds.), *Spill oil fingerprinting and source identification*, Academic Press, USA., **2006**

George, S. C.; Boreham, C. J.; Minifie, S. A.; Teerman, S. C. *Org. Geochem.* **2002**, *33*, 1293-1317

Halpern, H. I. *American Assoc. Pet. Geo.* **1995**, *79*, 801-815.

Head, I. M.; Jones, D. M.; Larter, S. R. Biological Activity in the Deep Subsurface and the Origin of Heavy Oil. Nature 2003, 426, 344−352

Kharrat, A.M., Indo, K., Mostowfi, F.; Energy Fuels 2013, 27, 2452−2457

Moldowan, J. M.; Fago, F. J.; Carlson, R. M. K.; Young, D. C.; van Duyne, G.; Clardy, J.; Schoell, M.; Pillinger, C. T.; Watt, D. S. *Geochim. Cosmochim.* **1991**, *55*, 3333-3353.

Mullins, O.C.; The Physics of Reservoir Fluids; Discovery through Downhole Fluid Analysis, Schlumberger Press, **2008**, Houston, TX

Mullins, O.C.; The Modified Yen Model, Energy & Fuels, **2010**, 24, 2179–2207

Mullins, O.C.; Zuo, J.Y.; Hammond, P.S.; De Santo, I.; Dumont, H.; Mishra, V.; Chen, L.; Pomerantz, A.E.; Dong, C.; Elshahawi, H.; Seifert, D.J.; **2014**, The dynamics of reservoir fluids and their substantial systematic variations, SPWLA Ann. Symp. Abu Dhabi

Peters, K. E.; Walters, C. C.; Moldowan, J. M. The Biomarker Guide: Biomarkers and Isotopes in Petroleum Systems and Earth History; Cambridge University Press: Cambridge, U.K., **2005**; Vol. 1 and 2.

Nelson, R.K., Kile, B.M., Plata, D.L., Sylva, S.P., Xu, L., Reddy, C.M., Gaines, R.B., Frysinger, G.S., Reichenbach, S.E., Tracking the weathering of an oil spill with comprehensive two-dimensional gas chromatography, Environ. Forensics, **2006,** 7, 33-44

Pomerantz, A.E.; Ventura, G.T.; A.M McKenna, J.A. Cañas, J. Auman, K. Koerner, D. Curry, Nelson, R.L.; Reddy, C.M.;Rodgers, R.P.; Marshall, A.G.; K.E. Peters, Mullins, O.C.; Combining Biomarker and Bulk Compositional Gradient Analysis to Assess Reservoir Connectivity, Org. Geochem. **2010**, 41 (8), pp. 812-821

Reddy, C.M., Nelson, R.K., Sylva, S.P., Xu, L., Peacock, E.A., Raghuraman, B., Mullins, O.C., Using GC×GC to identify and quantify olefin-based drilling oils in crude oils, Journal of Chromatography A, **2007,** 1148, 100-107.

Ruiz-Morales, Y.; Wu, X.; Mullins, O.C.; Electronic Absorption Edge of Crude Oils and Asphaltenes Analyzed by Molecular Orbital Calculations with Optical Spectroscopy, Energy & Fuels, 21, 944, (2007)

Schwatrz, F.P., Determinationof Temperature Dependence of Solubilities of Polycyclic Aromatic Hydrocarbons in Aqueous Solutions by a Fluorescence Method, Journal of Chemical and Engineering Data, **1977**, 22, 3, 273-277

Seifert, W. K.; Moldowan, J. M. *Adv. Org. Geochem.* **1980,** eds. A. G. Douglas and J. R. Maxwell. Pp. 229-237. Pergamon Press, Oxford

Thompson, K. F. M. *Geochim. Cosmochim.* **1983**, *47*, 303-316

Thompson, K F. M. *Org. Geochem.* **1987**, *11*, 573-590

Tissot, D.H., Welte, B.P.; Petroleum Formation and Occurrence: A New Approach to Oil and Gas Exploration, Springer-Verlag, Berlin, **1978**

Tong, H.Y., Karasek, F.W., Flame ionization detector response factors for compound classes in quantitative analysis of complex organic mixtures. Anal. Chem. **1984,** 56, 2124–2128

Welte, D. H.; Kratochvil, H.; Rullkotter, H.; Ladwein, H.; Schaefer, R. G. *Chem. Geo.* **1982**, *35*, 33-68

Zuo, J.Y.; Mullins, O.C.; Freed, D.E.; Dong, C.; Elshahawi, H.; Seifert, D.J.; Advances in the Flory-Huggins-Zuo Equation of State for Asphaltene Gradients and Formation Evaluation, Energy & Fuels, **2013**, 27, 1722–1735

Zuo, J.Y.; Jackson, R.; Agarwal, A.; Herold, B.; Kumar, S.; De Santo, I.; Dumont, H.; Beardsell, M.; Mullins, O.C.; A diffusion model coupled with the Flory-Huggins-Zuo Equation of State and Yen-Mullins model accounts for large viscosity and asphaltene variations in a reservoir undergoing active biodegradation, Energy & Fuels, **2015**, 29, 1447 −1460